iScience

CellPress
OPEN ACCESS

Perspective

Accelerating photo-thermal CO_2 reduction to CO, CH_4 or methanol over metal/oxide semiconductor catalysts

Kristijan Lorber[1,2] and Petar Djinović[1,2,*]

SUMMARY

Photo-thermal reduction of atmospheric carbon dioxide into methane, methanol, and carbon monoxide under mild conditions over suitable (photo)catalysts is a feasible pathway for the production of fuels and platform chemicals with minimal involvement of fossil fuels. In this perspective, we showcase transition metal nanoparticles (Ni, Cu, and Ru) dispersed over oxide semiconductors and their ability to act as photo catalysts in reverse water gas shift reaction (RWGS), methane dry reforming, methanol synthesis, and Sabatier reactions. By using a combination of light and thermal energy for activation, reactions can be sustained at much lower temperatures compared to thermally driven reactions and light can be used to leverage reaction selectivity between methanol, methane, and CO. In addition to influencing the reaction mechanism and decreasing the apparent activation energies, accelerating reaction rates and boosting selectivity beyond thermodynamic limitations is possible. We also provide future directions for research to advance the current state of the art in photo-thermal CO_2 conversion.

INTRODUCTION

The petrochemical industry relies on coal gasification and the steam reforming of natural gas to produce syngas, which is followed by the hydrogenation of CO to build valuable chemicals. Carbon from fossil sources is used as a building block; its burning provides the energy needed for these energy-demanding reactions. A transition from fossil fuel-dependent energy sources and utilization of atmospheric CO_2 is required to sustain the quality of human life and technological progress.

Photo-thermal catalysis uses light and thermal energy together to accelerate reactions. It is gaining momentum as a green and efficient pathway for converting intermittent photon energy into storable chemical energy (Wang and Domen, 2020), (Mateo et al., 2021). Because of endless sunlight abundance, light-assisted or preferably, light-driven large-scale photocatalytic reactions could play an important role in mitigating CO_2 emissions. Conversion of CO_2 to CO *via* the Reverse Water Gas Shift reaction (RWGS, $CO_2 + H_2 \leftrightarrow CO + H_2O$) or methane dry reforming reaction (DRM, $CH_4 + CO_2 \leftrightarrow 2H_2 + 2CO$), to methanol ($CO_2 + 3H_2 \leftrightarrow CH_3OH + H_2O$) or methane (Sabatier reaction, $CO_2 + 4H_2 \leftrightarrow CH_4 + 2H_2O$) are most relevant (Schwab et al., 2015).

Many thermally driven catalytic reactions are operated at non-ideal conditions (high temperature and pressure) to ensure sufficient productivities, leading to elevated energy input, expensive reactor design, and high CO_2 emissions.

By partially substituting thermal energy with photon energy, milder reaction conditions could be used to achieve or surpass the selectivity, conversion, and productivity of thermally driven catalytic reactions mentioned above, which are limited by thermodynamics (Gargiulo et al., 2019).

Nickel, copper, and ruthenium on suitable oxide semiconductors represent active and selective photocatalysts for CO_2 valorization to C1 chemicals under visible light illumination. Their affordability and scalable synthesis make them a good starting point for further chemical and structural optimization to improve performance, which could make them complementary to current industrial processes.

[1]Department of Inorganic Chemistry and Technology, Laboratory for Catalysts, National Institute of Chemistry, Hajdrihova ulica 19, SI-1000 Ljubljana, Slovenia

[2]University of Nova Gorica, Vipavska 13, SI-5000 Nova Gorica, Slovenia

*Correspondence: petar.djinovic@ki.si

https://doi.org/10.1016/j.isci.2022.104107

In photo-thermal reactions, several pathways which accelerate the catalytic turnover can occur simultaneously, namely: (i) Reduction and oxidation reactions driven by hot carriers: electron-hole pairs, formed after the promotion of valence band electrons to conduction band on the femtosecond time scale; (ii) Vibrational excitation of adsorbed species and reaction intermediates, induced by electromagnetic near-field enhancement (NFE). As the vibrational energy stored in the chemical bonds increases, they become progressively more destabilized. As a result, the energy barrier which remains to be overcome by thermal energy is decreased, leading to the acceleration of reaction rates; (iii) Non-emissive recombination of hot charge carriers resulting in heating of the catalyst and (iv) Over plasmonic metal structures (Al, Cu, Ag, Au) (Aslam et al., 2018), a resonant photo-induced collective oscillation of valence electrons can be established when the frequency of the photons matches the frequency of surface electron oscillations against the restoring force of positive nuclei. This is known as the localized surface plasmon resonance (LSPR) effect. It produces elevated electric fields on the metal surface, thereby yielding abundant energetic charge carriers (hot electrons and holes) through non-radiative decay. The hot electrons can assist in both bond activation and reaction intermediate conversion through transient electronic excitations (Wang et al., 2020).

The metal/oxide semiconductor composites are extensively researched and generally associated with economically viable and scalable synthesis. However, large bandgap energy and fast charge carrier recombination strongly limit their light-harvesting ability and efficiency in the utilization of hot charge carriers for the desired reactions (Wang and Domen, 2020).

When exposed to elevated temperatures (100°C–400°C), which is the usual practice in thermocatalytic CO_2 reduction reactions, the following phenomena are beneficial: Firstly, the thermal energy of the system increases with increasing temperature (8.617×10^{-5} eV for each degree K), resulting in higher energy of electrons in the ground state. Consequently, less energetic photons can be used to excite electrons across the bandgap, thus generating hot carriers. An increase in intrinsic carrier concentration correlates with elevated temperature and in case of indirect bandgap semiconductors, the charge carrier recombination decelerates as temperature increases (Johnston and Ahrenkiel, 1999).

Secondly, in reducing atmospheres (CO_2 reduction reactions generally require conditions with excess H_2), partial reduction of oxide semiconductors occurs ($MO_x + H_2 \rightarrow H_2O + MO_{x-1}$). This substantially alters their chemistry and electronic structure. It broadens the range of absorbed wavelengths compared to ambient temperature in air and generates deep or shallow traps. This aspect is often overlooked and seemingly non-perspective metal/oxide semiconductor catalysts can transform into efficient photocatalytic workhorses (Tan et al., 2020; Xie et al., 2020; Lorber et al., 2022).

Bandgap alteration is the most extensively explored over oxygen-deficient "black titania," where on reduction, the bandgap reduces from 3.2 eV to approximately 1.6 eV (Han et al., 2016). Besides TiO_2, several other oxide semiconductors, such as ZnO (Divins et al., 2021) CeO_2 (Zhang et al., 2020), MnO_3 (He et al., 2019) and WO_3 (Shi et al., 2019), which constitute active catalyst supports in CO_2 reduction catalysis, are susceptible to partial reduction under mild conditions.

The role of metal nanoparticles (Cu, Ni, Co, Pt, Au, etc.) is to act as an electron sink (prolonging charge separation) and activation of reactants (Li et al., 2019).

RESULTS AND DISCUSSION

CO_2 activation

It can take place both on metal and metal oxide surfaces. CO_2 is a very stable molecule with a C=O bond dissociation energy of about 750 kJ/mol. The activation of adsorbed CO_2 occurs by electron transfer from the surface to the CO_2 molecule. This requires the alignment of the Fermi energy levels of the metal and the Lowest Unoccupied Molecular Orbital (LUMO) of CO_2. Electron transfer to LUMO results in the formation of CO_2^- surface species, which is a bent anion (Ansari and Park, 2012). This causes weakening and elongation of the C=O bond, making its dissociation easier.

Surface defects, such as oxygen vacancies are among the most reactive sites on the surfaces of metal oxides. Upon the creation of the oxygen vacancy (loss of an oxide anion, O^{2-}), the neighboring cations attain a partly reduced state due to charge re-distribution ($Ce^{4+} \rightarrow Ce^{3+}$, $Ti^{4+} \rightarrow Ti^{3+}$, *etc.*). Upon the interaction of

the CO_2 molecule with such a surface motif, the increased electron density over the partly reduced metal favors electron donation to CO_2 forming the bent anion, whereas the adjacent oxygen vacancy acts as a sink to detach and accommodate the oxide anion, thus replenishing the vacancy. As a result, CO_2 dissociation barrier is diminished and can be achieved under mild conditions (Liu et al., 2012).

The group of Ozin discovered the important role of Frustrated Lewis acid–base pairs (FLPs) for CO_2 activation with an $In_2O_{3-x}(OH)_y$ catalyst (Hoch et al., 2014). Lewis basic hydroxide groups and Lewis acidic indium atoms located adjacent to the oxygen vacancy, similar to molecular FLPs, work in a concerted manner to dissociate H_2 and activate CO_2.

H_2 activation

This occurs on metallic surfaces. The process of breaking the H-H bond is known to proceed without an activation barrier on transition metals (Ni, Cu, Ru), whereas with noble metals this is an activated process requiring external energy input (Darling and Holloway, 2003). The reason for this is due to the availability of s → d electron transfer in these metals and the concomitant weakening of the Pauli repulsion, normally exhibited when the closed-shell H_2 molecule begins to interact with the s orbitals of the metal.

CH_4 activation

Due to the symmetry of the methane molecule, difficult polarizability and high energy of C—H bonds (476 kJ/mol) methane activation require the use of catalysts and high temperatures (>500°C). Methane activation usually takes place on metallic surfaces such as Pt, Ru, Ni, Co, and Rh. However, compared to continuous metallic surfaces, metal-support interface sites provide substantial benefits in terms of alleviation of the methane activation due to the dual nature of the active perimeter.

Hensen et al.(Su et al., 2018) reported an oxygen-deficient Pd-doped CeO_2 (111) surface as highly active for methane dissociation. Similar structures also exist for Ni and Pt-doped ceria surfaces, enabling methane activation at room temperature (Lustemberg et al., 2016). Focusing on the activation barrier for C–H bond cleavage, supported Ni nanoparticles together with strong Ni-support bonding and charge transfer at the step edge are key to the high catalytic activity. They enable a decrease in the activation barrier from about 86 kJ/mol, characteristic for continuous metal surfaces to 9 kJ/mol, which approaches a spontaneous, non-activated process (Lustemberg et al., 2021). Later in discussion we discuss how light contributes to reactant activation and acceleration of reaction rates.

We can control products distribution using different active metals and supports, which favor the reaction intermediates leading to the desired reaction product. Also, the H_2/CO_2 ratio, as well as temperature and pressure can shift selectivity from CO to CH_4 over the same catalyst. However, in photo-thermal chemistry, we have additional leverage which is light.

Upon illumination, photo-excited hot carriers are generated in the semiconductor, which migrates from the semiconductor to the supported metal nanoparticles and accumulates on their surface. Increased density of highly energetic electrons on the metal leads to higher frequency and probability for their injection into the antibonding orbital of the adsorbed species and reaction intermediates, which accelerates their activation.

It should be noted that the direction of hot carrier migration is not always from the semiconductor to the metal, but is influenced by the position of the Fermi levels of (both) catalyst constituents in contact, the type of junction that forms on the interphase (Schottky or Ohmic) and the possible plasmonic effect on metal (Li et al., 2019). The group of Halas showed that in plasmonic metal structures such as Au nanoparticles, surface plasmons excited in the Au nanoparticle decay into hot electrons. In this transient state, hot electrons can transfer into the H_2 molecules adsorbed on the Au nanoparticle surface, triggering dissociation (Mukherjee et al., 2013).

Illumination improves the formation of oxygen vacancies in reducible oxide semiconductors in the presence of hydrogen (Lin et al., 2017). Higher abundance of vacancy sites means more active sites are available for CO_2 dissociation. Also, the accumulation of the hot holes that diffuse to the surface of the oxygen-deficient semiconductor can help with the incorporation of the O^{2-} anion into the oxygen vacancy site, thus accelerating its regeneration (Lorber et al., 2022).

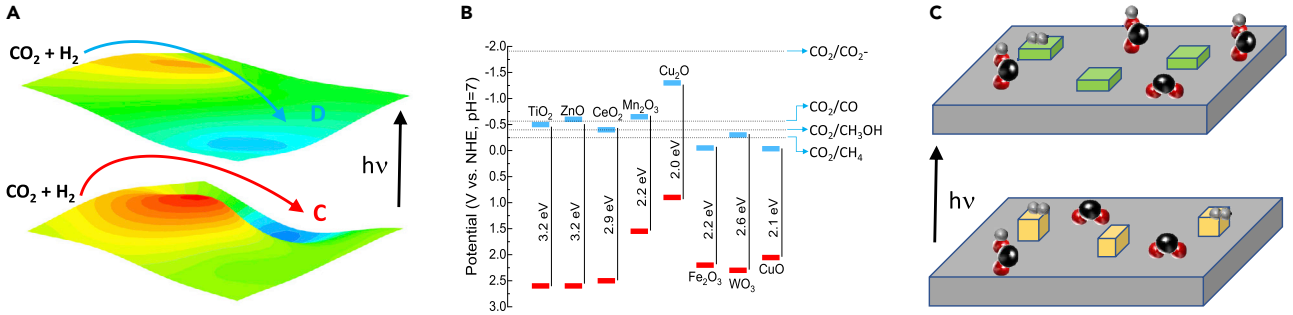

Figure 1. Potential energy landscape, energy levels of conduction and valence bands and light-induced restructuring of catalysts

(A) Different potential energy landscapes during thermal (ground state) and photo-thermal reactions (excited state) can influence product distribution. Inspired by Gargiulo et al.(Gargiulo et al., 2019).

(B) Valence (red) and conduction band (blue) potentials of selected oxide semiconductors and the corresponding redox potentials of CO_2 reduction reactions. Inspired by Chang et al.(Chang et al., 2016).

(C) Schematic drawing of illumination causing metal nanoparticles restructuring and changing their oxidation state (yellow and green cuboids), together with a change in surface adsorbed species. Black sphere = carbon atom, red sphere = oxygen atom, grey sphere = hydrogen atom.

Upon the illumination of the defective $In_2O_{3-x}(OH)_y$ surfaces supporting the FLP sites, the electronic transitions due to Metal to Ligand Charge Transfer (MLCT) are more intense than transition due to Ligand to Metal Charge Transfer (LMCT). This will cause a net increase in electronic charge on OH and a decrease in electronic charge on the surface Indium atom. As a result, the Lewis basicity and Lewis acidity are enhanced in the excited state, resulting in higher reactivity of the FLPs for CO_2 dissociation (Ghuman et al., 2016).

In addition to the above-described pathways, absorbed light can cause strong amplification of the electromagnetic near field. This can result in the deposition of vibrational or rotational energy into the adsorbed species, causing destabilization of their bonds (Asapu et al., 2019).

If recombination of hot carriers takes place in a non-emissive manner, the excess energy is dissipated in terms of heat, causing heating of the active sites.

Next, we discuss how light affects selectivity in photo-thermal reactions.

In the excited state, the potential energy landscape is different compared to the ground state in the dark (Figure 1A). The origin of this phenomenon is the delocalization of electrons and population of energy states which are empty under thermal conditions (in the dark). As a result, the minimum energy pathway between reactants and products can be noticeably different, leading to altered selectivity (Gargiulo et al., 2019).

The different electrochemical potentials for CO_2 reduction reactions (to CO, methanol, methane, *etc.*) and CB potentials of suitable oxide semiconductors can be utilized to guide selectivity. Direct one electron CO_2 reduction is highly unfavorable as it requires a potential of −1.9eV vs NHE, which cannot be met by narrow bandgap semiconductors. However, the reduction potential for proton-assisted multi-electron CO_2 reduction is much lower and can be reached by several semiconductors, Figure 1B. Namely, if one wants to promote methanol selectivity ($CO_2 + 6e^- + 6H^+ \rightarrow CH_3OH + H_2O$, −0.38 eV) over selectivity for CO ($CO_2 + 2e^- + 2H^+ \rightarrow CO + H_2O$, −0.52 eV), the CB potential of a semiconductor should be more negative than the potential of CO_2/CH_3OH, but more positive than the CO_2/CO reaction.

For strongly absorbing (plasmonic) metals, light can induce dramatic changes in their oxidation state. This was observed for copper, where on illumination a transition from Cu^{1+} to Cu^0 takes place, resulting in a notable shift of reaction selectivity (Marimuthu et al., 2013). Plasmonic nanoparticles (Cu and Ag) can also restructure and grow from illumination-induced localized heating (Kumari et al., 2021), (Molotskii, 2009). This can change the distribution of exposed crystal facets and ratio between terrace, kink, and edge sites, affecting selectivity (Van Hardeveld and Hartog, 1969), (Xiong et al., 2021). Also, the distribution and activation of specific reaction intermediates can be influenced by light through selective electronic injection into vacant adsorbate antibonding orbitals, leading to accelerated reaction rates or altered product distribution (Figure 1C) (Tan et al., 2020).

In the following section, photo-thermal CO_2 reduction reactions over transition metal@oxide semiconductor catalysts are presented to showcase the effects of visible light on reaction rates and product selectivity.

The DRM reaction produces CO-rich syngas and is typically performed at high temperatures (700–1000°C). Operating the DRM reaction at low temperatures (below 500°C) would greatly decelerate the metal sintering and avoid deactivation and coking of catalyst. However, poor selectivity due to kinetic dominance of RWGS is expected at low temperatures. The rate-determining step (RDS) is methane activation, which is accelerated on small metal ensembles (Vogt et al., 2020). The reaction has several drawbacks: (i) carbon accumulation on the catalyst which prevents long term stability (Vasiliades et al., 2017) and (ii) kinetically much faster RWGS reaction, which converts a large fraction of H_2 to water (Djinović et al., 2011).

Nanoclusters of nickel, dispersed over high surface-area CeO_2 represent an exceptionally active catalyst that can activate methane already at room temperature (Lustemberg et al., 2016).

In recent years, several studies emerged of combined photo-thermal and photo-catalytic DRM reactions (Han et al., 2016, 2019; Liu et al., 2016; Song et al., 2018a, 2018b; Shoji et al., 2020a; Zhou et al., 2020). The tested catalysts were based on noble metals (Au, Pt and Pd) (Vogt et al., 2020), (Wei and Iglesia, 2004), supported on TiO_2, TaON or $SrTiO_3$ as light-absorbing semiconductors. Rh supported on TiO_2 and $SrTiO_3$ were studied in combined photo-thermo-catalytic mode, illuminated by a Hg-Xe lamp (Cho et al., 2020), (Shoji et al., 2020b). The authors reported methane conversion and H_2 selectivity beyond the thermodynamic equilibrium at temperatures below 450°C. Photocatalytically assisted DRM reaction using visible light was probed for Pt/TiO_{2-x} (Han et al., 2016), $Au\text{-}Pd/Al_2O_3$ (Liu et al., 2016), $Au\text{-}Pt/SiO_2$ (Song et al., 2018). Over Pt/Al_2O_3, no benefit of visible light illumination was observed compared to thermocatalytic reaction, the catalyst exhibited low catalytic activity (5mmol CH_4/g_{cat}*h at 450°C). Over Pt/TiO_{2-x} up to 50% boost in methane and CO_2 conversion, compared to thermocatalytic reaction was achieved at 700°C. At 450°C under visible light illumination, it converted 30 mmol CH_4/g_{cat}*h (Han et al., 2016). The $Au\text{-}Pt/SiO_2$ and $Au\text{-}Pd/Al_2O_3$ catalysts converted 0.28–0.32 mmol CH_4/g_{cat}*h at 450°C when illuminated with 0.21 W/cm^2 visible light. Catalyst illumination boosted catalytic performance by approximately 15%.

During the DRM reaction using $2Ni/CeO_{2-x}$, nickel is present in the form of metallic nanoparticles decorating the surface of partially reduced ceria (Zhang et al., 2020). The H_2 and CO rates achieved under photo-thermal conditions are about 10- and 30-fold higher compared to values obtained in the dark at 360°C, respectively (Figure 2). Also, the H_2/CO ratio, which reflects reaction selectivity, was improved to values beyond the thermodynamic equilibrium. The apparent activation energies (Ea) for H_2 and CO under illumination decreased to one-quarter of the values in dark, indicating a strongly modified reaction mechanism with a substantial decrease of the energy barriers related to the rate-determining step of reaction (methane activation on nickel). The photo-thermal DRM reaction can be sustained at temperatures that are 180°C lower compared to the thermally driven catalytic reaction (Lorber et al., 2022).

Focal points to address in photo-thermal dry reforming reaction reaction

Design of transition metal@semiconductor photocatalysts focusing on accelerating the RDS of the reaction: C-H bond activation in methane by direct dehydrogenation (on the metallic sites) and oxygen assisted pathways (at partly oxidized metal centers at the metal-support interface) (Xie et al., 2017).

The impact of the RWGS reaction which decreases H_2 selectivity should be minimized by weakening the H_2 adsorption energy. Active metal modification via alloying and use of visible light excitation (hot carrier energy transfer and electron-vibrational scattering) to accelerate the associative desorption of H_2 appear as possible strategies (Zhou et al., 2020), (Zhou et al., 2019).

Methanol synthesis *via* hydrogenation of CO_2 is performed at elevated pressures (30–100 bar) and temperatures between 230 and 300°C using a $Cu\text{-}ZnO_x\text{-}AlO_x$ catalyst (Ott et al., 2012). Copper, which is the major component of the catalyst (~30–60 wt %) is present in the metallic form during reaction (Zabilskiy et al., 2020), coexisting with finely dispersed and oxygen-deficient ZnO_x. This suggests that the catalyst could be photo-thermally excited using visible light (Cu exhibits a localized surface plasmon resonance maximum at ~590 nm) (Xie et al., 2021).

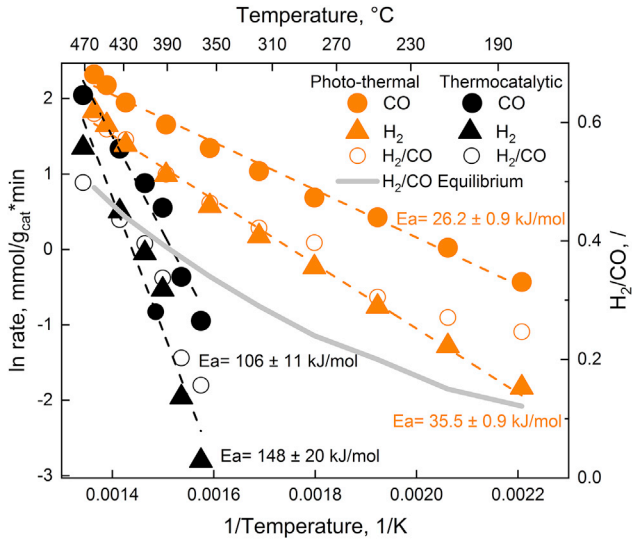

Figure 2. Reaction rates and selectivity during photo-thermal methane reforming reaction

The H_2 and CO rates with corresponding H_2/CO ratios in thermocatalytic (black symbols) and photo-thermal DRM reaction (orange symbols) over 2 wt % Ni/CeO_{2-x} catalyst. The grey line represents the H_2/CO ratio determined by the thermodynamic equilibrium (Lorber et al., 2022).

Due to the exothermic nature of the reaction, equilibrium-limited conversion, and high activation energy barrier for CO_2 hydrogenation, the process is a compromise between reaction temperature and high pressures to achieve a sufficient selectivity and production rate. High pressures and low temperatures are preferred to minimize the main competing side reaction (RWGS), which lowers the methanol selectivity. Cu, Pd, In or Ga-based catalysts, supported on ZrO_2, CeO_2, ZnO, TiO_2 give the highest methanol yields (Porosoff et al., 2016). From a mechanistic point of view, the catalytic hydrogenation of CO_2 to methanol can occur directly or indirectly with the participation of CO formed through the RWGS reaction (Kondratenko et al., 2013). The active sites should bind the formate intermediate with sufficient strength to prevent premature CO desorption and also prevent total hydrogenation to methane (Graciani et al., 2014). Synergy of Cu and ZnO at the interface represents the active site which facilitates methanol synthesis via the formate intermediate (Nakamura et al., 2017). Overall, methanol synthesis rates are limited by methoxy (CH_3O*) formation at low CO_2/(CO + CO_2) ratios and by CH_3O* hydrogenation in CO_2-rich feeds. CH_3O* hydrogenation is the common slow step for both the CO and the CO_2 methanol synthesis routes (Grabow and Mavrikakis, 2011).

Solar methanol production at a rate of 0.06 mmol/g_{cat}*h at 50% methanol selectivity and atmospheric pressure with rod-like $In_2O_{3-x}(OH)_y$ nanocrystals was discovered by the Ozin group (Wang et al., 2018). This is more than two orders of magnitude higher compared to all previous photocatalytic attempts (Wang et al., 2018). However, compared to the state of the art performance in thermocatalytic reaction (220 mmol/g_{cat}*h) (Bansode and Urakawa, 2014), the gap for improvement remains huge (taking into account the different reaction conditions). The very limited photocatalytic methanol synthesis experiments published to date have hardly touched on the potential of this reaction.

Wang et al.(Wang et al., 2019a) analyzed visible light (0.58 W/cm^2) as an external stimulus to boost methanol synthesis using Cu/ZnO catalysts at atmospheric pressure. Experimental and theoretical analyses suggest that hot electrons were photo-excited by LSPR on Cu nanoparticles and as such the photo-excited hot electrons could transfer to ZnO. The hot electrons on Cu and ZnO synergistically facilitated the activation of the reaction intermediates. Consequently, the activation energy was reduced by 40% and the methanol formation rate was accelerated by 54%. Interestingly, light had a negligible effect on the methanol selectivity, which dwelled at about 8% at 220°C.

The group of Amal analyzed photo-thermal methanol synthesis using a commercial $CuZnAlO_x$ catalyst (Xie et al., 2020). They stress that an associative ZnO band-gap excitation and copper plasmonic excitation using UV-Vis wavelengths cooperatively promotes methanol-production at the Cu–ZnO interface.

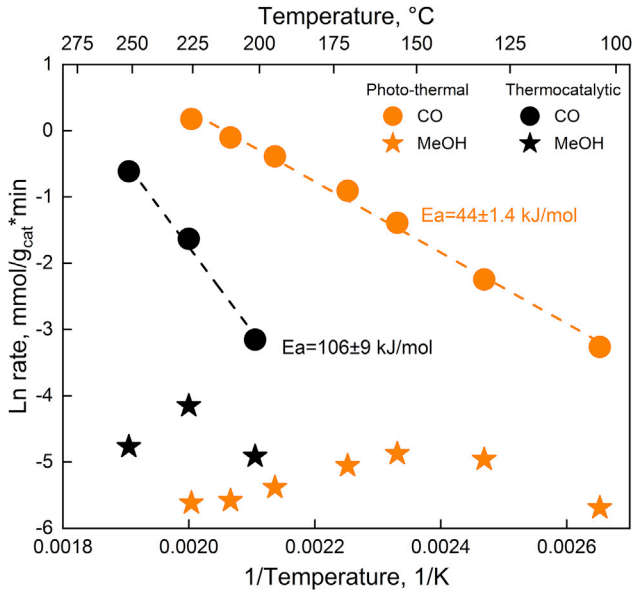

Figure 3. Reaction rates and selectivity during photo-thermal CO_2 reduction to methanol

CO and methanol rates during CO_2 hydrogenation over a commercial Cu-ZnO_x-Al_2O_3 catalyst (ICI Katalco 51–8 by Johnson Matthey) in thermocatalytic and photo-thermal mode.

Specifically, illumination activates surface adsorbates (formate conversion and hydrogen molecule activation), thus giving rise to the observed photo-thermal activity. Conversely, selective excitation of individual components (UV for ZnO or Vis for Cu) favors only CO production.

In the thermally driven mode using the commercial Cu-ZnO_x-AlO_x catalyst, carbon monoxide is the dominant reaction product (Figure 3). Methanol selectivity follows a volcano-shaped curve as a result of unfavorable thermodynamics at high temperatures and low reaction kinetics at low temperatures. In the photo-thermal mode, the activity of the catalyst is greatly improved (15-fold higher CO rate at 200°C) and catalytic activity is sustained until 100°C. As in the case of the thermally driven reaction, methanol selectivity follows a volcano-shaped trend. At identical CO_2 conversions, the maximum methanol selectivity reaches 15% at 200°C in thermally driven and 3% in the photo-thermal mode at 160°C, respectively. Due to operation at ambient pressure (1 bar), the methanol selectivity is low. Illumination of the catalyst with visible light causes the acceleration of the RWGS pathway at the expense of the methanol forming pathway.

Focal points to address in photo-thermal methanol synthesis

To bypass thermodynamic restrictions and produce methanol with high rates at low temperatures (below 200°C) and low pressures (1–10 bar), maximizing the efficiency of non-thermal energy input is crucial. Experiments with high irradiances and suitable spectral emission are required (Xie et al., 2020). Alternatively, ordered mesoporous semiconductor supports containing plasmonic metal particles with homogeneous spatial distribution could give good results. Namely, illumination of arrays of plasmonic metallic nanoparticles will strengthen their collective LSPR oscillation, which is known for near electromagnetic field enhancement of x10,000-100,000 compared to incident illumination (Aslam et al., 2018). As a result, intense photo-catalytic rate acceleration could be achieved.

The RWGS reaction is of particular interest due to the direct use of CO as a feedstock in many important industrial processes such as CH_3OH synthesis and the Fischer–Tropsch process to yield liquid fuels. Most extensively researched RWGS catalysts are based on Cu, Pt, or Fe (Schwab et al., 2015).

Metal-support interface is the reactive perimeter (Kopač et al., 2020) and the reaction proceeds via the formate and/or carbonate mechanisms, which are still debated. On reducible supports such as TiO_2 and CeO_2, the redox mechanism is dominant and CO_2 dissociation is the RDS (Wilkinson et al., 2016). Strong

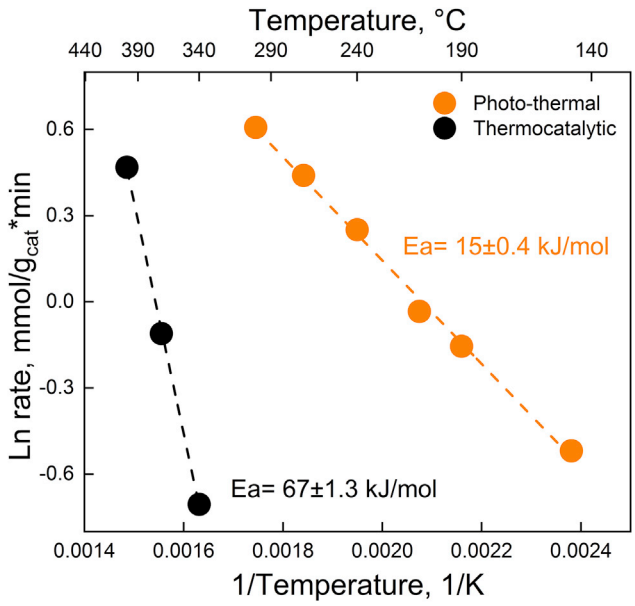

Figure 4. Reaction rates during photo-thermal reverse water gas shift reaction

CO rate during RWGS reaction over 10 wt % Cu/CeO_{2-x} catalyst in thermocatalytic and photo-thermal modes.

CO binding to metallic sites (Pt and Ni) overpopulates them, making them inaccessible for H_2 activation (Williams et al., 2017), which results in absence of low-temperature activity (below 200°C).

Direct catalytic activation of CO_2 on copper is energetically very demanding and is greatly accelerated in substantial H_2 excess (Vovchok et al., 2020). Also, low-temperature RWGS activity is hampered by strongly adsorbed CO on the catalyst, causing blockage of the active sites (Williams et al., 2017). Thus, innovative pathways for accelerating RWGS rate under H_2 lean conditions and at low temperatures (below 200°C) are highly desired.

Yang et al.(Yang et al., 2022) report that the RWGS catalytic activity of 5 %Cu/CeO_2 catalyst upon visible light illumination increases by 30 % at 250°C. They used a combination of *in situ* DRIFTS, EPR, and XPS characterization to demonstrate that under visible light irradiation, the LSPR produced by Cu nanoparticles stimulates hot electrons transfer to ceria, causing destabilization and desorption of bidentate formate and linear-CO intermediate species. Moreover, the spillover of H_2 from Cu to CeO_2 surface is also affected by light due to the observed regeneration of oxygen vacancies on the CeO_2 surface, which positively influences the CO yield. The Amin group (Tahir et al., 2015) analyzed Au-In/TiO_2 deposited over alumina monoliths under UVC illumination. In addition to CO, methane and small amounts of C2-C3 olefins and paraffins were detected among reaction products (Tahir et al., 2015). However, no benchmarking with thermo-catalysis or contribution of the photo-thermal effect was provided. The group of Ma (Song et al., 2020) investigated the tunable selectivity in photo-thermal RWGS over a series of Fe-based catalysts when illuminated by Xe light at 2.05 W/cm^2 intensity. The Fe_3O_4 catalyst steered selectivity only toward CO, with CO productivity of 11.3 $mmol/g_{cat}$*h, whereas the θ-Fe_3C phase produced methane with selectivity above 97%.

In thermo-catalytic RWGS reaction under H_2 lean conditions, the $10Cu/CeO_{2-x}$ catalyst shows no activity below 340°C (Figure 4). However, in the photo-thermal mode, CO formation is observed as low as 150°C. In addition to extending the range of working conditions towards lower temperatures by almost 200°C, which was previously possible only on Au/TiO_2 catalysts in excess of H_2 (Kyriakou et al., 2017), the apparent activation energy is decreased from 67 to 15 kJ/mol. This reveals a very strong effect of visible light on alleviating the energetic barriers for CO_2 reduction.

Focal points to address in photo-thermal reverse water gas shift reaction reaction

Enabling light-assisted RWGS reaction under H_2 lean conditions and mild conditions using novel photocatalysts. Decoupling of the RWGS and methanation reaction pathways by light-induced selective destabilization of surface adsorbates resulting in the extended range of reaction conditions enabling total CO selectivity on metals such as Fe and Ni.

CO_2 hydrogenation to methane (Sabatier reaction) is the backbone of the *power to gas concept*, which produces synthetic natural gas using nickel or ruthenium-based catalysts. In view of thermodynamics, the reaction is highly favorable with large negative values of enthalpy and Gibbs free energy. At the same time, the involvement of eight electrons ($CO_2 + 8e^- + 8H^+ \rightarrow CH_4 + 2H_2O$, −0.24 eV) makes it highly kinetically limited. The reaction is catalyzed by Ni, Fe, Rh, and Ru (Boll et al., 2011). Catalysts based on Ru are generally most active and less susceptible to fouling by carbon, their activity stretches to temperatures below 200°C (Vrijburg et al., 2019). The support plays an important role through the adsorption of OCH_x intermediates ($1 < X < 3$), which undergo sequential hydrogenation via hydrogen spillover, originating from H_2 dissociation over metallic nanoparticles. Al_2O_3, ZrO_2, SiO_2, TiO_2, $CeZrO_2$, and CeO_2 are the most extensively investigated supports. By decorating nickel with Mn^{2+} to form Ni-MnO nanoparticles supported on TiO_2, the group of Hensen was able to reach the intrinsic activity of Ru/TiO_2 by promoting CO_2 adsorption and activation (Vrijburg et al., 2019). The selectivity for methane is rivaled by CO, selectivity for the latter depends on the reaction temperature, active metal and support interface, as well as CO_2: H_2 feed stoichiometry (Kattel et al., 2017). In general, two mechanisms are discussed: (i) CO_2 dissociation to yield a CO intermediate with subsequent CO methanation and (ii) direct CO_2 hydrogenation toward CH_4 (Solis-Garcia et al., 2017), (Aldana et al., 2013). The CO intermediate in the first mechanism may either be formed through direct CO_2 dissociation, or via formate decomposition (Karelovic and Ruiz, 2013). Recent studies on Ni-based catalysts have highlighted the influence of Ni particle size (Vogt et al., 2019) and the support on the CO_2 methanation pathways (Aldana et al., 2013), (Muroyama et al., 2016), (Pan et al., 2014).

Meng et al. (Meng et al., 2014) investigated photo-thermal CO_2 hydrogenation to methane in a batch reactor illuminated by a 300W Xe lamp over a series of transition metals supported on alumina. They achieved above 98% selectivity for methane with Ni, Ru, Rh, Co, and Pd. In contrast, CO selectivity of 36, 84, and 95% was obtained with Ir, Pt, and Fe, respectively. Recently, the group of Amal (Tan et al., 2020) used *in situ* DRIFTS-SSITKA to identify that formate (HCO_2) decomposition is the RDS of the reaction. This reaction intermediate is destabilized during illumination with visible light (532 nm), resulting in an up to 8-fold acceleration of CO_2 hydrogenation rate to methane over NiO_x/La_2O_3-TiO_2 catalyst.

The group of Dai investigated the methanation of CO_2 with $Ru/TiO_{(2-x)}N_x$ in thermal and photo-thermal modes using visible light irradiation ($435 < \lambda < 465$ nm) (Lin et al., 2017). They found that $Ru/TiO_{(2-x)}N_x$ exhibits higher catalytic activity than Ru/TiO_2 under visible light irradiation and in the dark. The benefit of visible light is much more significant on $TiO_{(2-x)}N_x$ (the CO_2 TOF increased from 8 to 18 h^{-1} at 190°C). Based on the results of chemisorption, temperature-programmed surface reaction, XPS, and photocurrent analyses, the photo-effect originates mainly from (i) the $TiO_{(2-x)}N_x$ itself is able to absorb CO_2 and convert it to CO, as the intermediate of CO_2 methanation reaction. Visible light amplifies this process by forming much more abundant oxygen vacancies in $TiO_{(2-x)}N_x$. (ii) The photo-generated hot electrons can transfer from $TiO_{(2-x)}N_x$ to Ru nanoparticles, resulting in the increase in the surface electron density of Ru. This leads to promoted adsorption and activation of CO_2.

With the $3Ru/TiO_2$ catalyst, methane is produced with selectivity above 90% at 400°C, along with CO as the side product (Figure 5). Methane selectivity increases with decreasing temperature and reaches 100% below 330°C. In the photo-thermal mode, a positive effect on methane rate and simultaneously, a negative one on CO rate is observed. This is especially important due to the necessity of CO absence in the natural gas grids due to its high toxicity. The Ea for methane decreases more compared to Ea for CO, suggesting that the methane reaction pathway is more sensitive to light. Furthermore, light can be used to steer CO and CH_4 selectivity without changing the catalyst temperature (Figure 4, inset): progressively increasing irradiance from 0 to 790 mW/cm^2 decreased the CO selectivity from 9 to 3%.

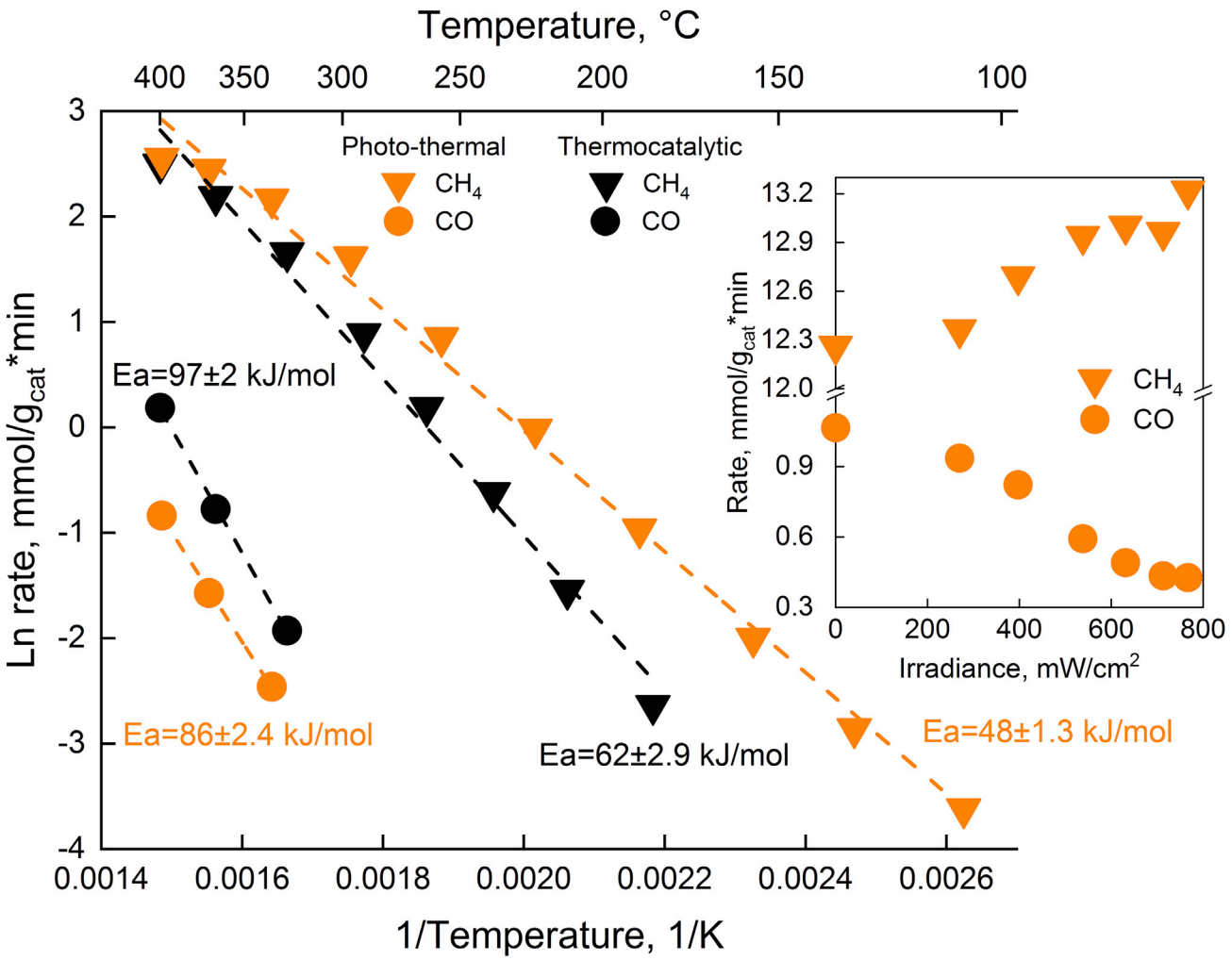

Figure 5. Reaction rates during photo-thermal Sabatier reaction

Sabatier reaction over 3 wt % Ru/TiO_2 catalyst in thermocatalytic and photo-thermal modes. Inset showing effect of irradiance on CH_4 and CO rates at a constant catalyst temperature of 340°C.

Focal points to address in photo-thermal Sabatier reaction

Systematic analysis of formation and light-induced decomposition of the surface formate species via temperature programed and *in situ* spectroscopic analyses. Decoupling of the RWGS and methanation pathways via light-induced selective destabilization of surface adsorbates.

OUTLOOK AND FUTURE PROSPECTS

To improve our understanding of photo-thermal catalysis and incorporate it more quickly and efficiently into the existing chemical processes, the following aspects should be systematically addressed and interconnected: experimentation, characterization, and theoretical computation.

Experimentation

Catalytic CO_2 reduction reactions in continuous flow mode are preferred due to much better mass transfer and heat management, compared to the more generally used batch reactor experimentation without stirring. When determining the catalyst layer geometry and illumination, one should consider a very limited penetration depth of light into solid materials (usually below 100 nm). A thin catalyst layer maximizes the fraction of irradiated material. This way, the majority of the analyzed catalyst can actually participate in the photo-thermal reaction.

Thermo-catalytic and photo-catalytic contributions are analyzed as lumped parameters (reaction rates, conversion, and selectivity). To decouple them, photon flux to the catalyst should be sufficient to make the photo-catalytic contribution stand out compared to thermal contribution. Let's consider the RWGS reaction which requires 2 electrons per turnover. If we want to photocatalytically enable the reaction rate of 1 μmol CO/min, then one should provide at least $2*10^{19}$ photons per second.

Suitable control experiments are required to correctly and convincingly assign the positive illumination effect to photocatalysis and not inaccurate temperature measurement (Mateo et al., 2021). The influence of light intensity on the photocatalytic rate can be a powerful tool to analyze the reaction mechanisms in photo-thermal processes (Mateo et al., 2021). Four different kinetic categories were classified in photo-thermal catalysis: sublinear (rate $\propto I^n$, $n < 1$), linear (rate $\propto I$), superlinear (rate $\propto I^n$, $n > 1$) and exponential (rate $\propto e^{f(I)}$) (Kale et al., 2014). The exponential dependence is characteristic for thermally driven reactions, which is consistent with the Arrhenius law.

Important information on the occurring photocatalytic mechanisms and the role of photocatalytic components can be achieved by preferential (selective) excitation of only one photoactive component. Wavelength-dependent studies can achieve this by using photons that have suitable energy to drive bandgap or intra bandgap excitation of individual components present in the catalyst.

The benchmarking of photocatalytic materials' efficiency is difficult and not widely practiced, which should be to some extent systematized, as proposed recently by Melchionna and Fornasiero (Melchionna and Fornasiero, 2020). The efficiency of the photocatalyst is related to the fraction of light that is effectively used by the catalyst to perform the chemical conversion. The concept of quantum yield (QY) encounters a problem for heterogeneous catalytic systems, as the number of photons that have been actually absorbed by the material is unknown, due to the additional scattering and reflection phenomena. For this reason, the concept of apparent quantum yield (AQY) is more appropriate. The AQY refers to the number of incident photons of a given wavelength per time and volume that reach the inside of the photoreactor (Kisch and Bahnemann, 2015).

Characterization

Precisely engineered photocatalytic materials, optimized for the specific reaction can be constructed through the understanding of the basic physical phenomena, occurring during light-matter interactions under relevant reaction conditions. Metals and oxide supports (semiconductors) that exhibit intrinsic (thermocatalytic) activity for the desired CO_2 reduction reactions should be the starting point of research. These materials enable adsorption and activation of reactants, and the formation of suitable reaction intermediates and transition states leading to the desired product. Having a material with a suitable position of VB and CB means nothing if there is negligible interaction of its surface with the (gaseous) reactants.

In situ characterization is steadily becoming a foundation in heterogeneous catalysis. In photocatalytic experimentation, it is additionally complicated due to the required illumination of the analyzed catalytic surface. As a result, purpose-built photo-catalytic chambers are required for the combined *in situ* DRIFTS, XPS, Raman, XRD, and XAS experimentation (Agostini et al., 2018; Collado et al., 2018; Muñoz-Batista et al., 2018; Weckhuysen Research Group Website, 2021). This way, light-induced changes in the structure of adsorbed surface species (reaction intermediates and spectators) (Marimuthu et al., 2013), oxidation state (Marimuthu et al., 2013), (Wang et al., 2019b), and shape of metal (Lee et al., 2018) and semiconductor, as well as their long- and short-range structural changes are accessible.

Steady-State Isotopic Transient Kinetic Analysis (SSITKA) experiments employ a combination of DRIFT and MS techniques. They can analyze the dynamics of surface species and formation of gaseous reaction products in both thermo catalytic and photo-thermal modes. This way, the light-induced changes to the reaction mechanism and its connection to the catalyst structure can be correlated.

Theoretical calculations

The ultimate goal of first-principles theoretical simulations is to solve the Schrödinger equation, which describes the system of *N* electrons and *M* nuclei. As a result, it is possible to compute the electrodynamic properties for bare semiconductors and metal nanoparticles, or their composites. The results can be

used to analyze the effect of the metal particle shape, size, and alloying on extinction, scattering, and near field strength and spatial distribution as a function of wavelength and temperature (He et al., 2021; Lorber et al., 2022). This can be implemented to guide the synthesis and minimize experimental trial and error, as well as to complement experimental characterization.

Tailored for ground-state electronic calculations, DFT is useful for calculating bulk properties (band structure, bandgaps, the electron and hole effective masses, dielectric constants, optical properties), alloy properties, and band alignments (Oba and Kumagai, 2018). Upon post-processing (projected) density of states, schematic representations of molecular orbitals, density difference maps, charge distribution and transfer, recombination rate, optical spectra, etc. are discovered (Meng et al., 2019).

However, pure DFT is ill-suited for explaining photocatalysis because it relies on ground electron density and cannot describe the excited electronic states. Nevertheless, its use in photo-catalysis is commonplace. Such applications are not entirely irrelevant, as thermo-catalytic pathways contribute a non-negligible part of the activity even under irradiation, thus allowing us to identify the relevant slow elementary steps using DFT (Martirez et al., 2021). More importantly, ground-state properties of the catalyst correlate strongly with its photocatalytic activity, warranting their use in material screening and catalyst discovery. Several large computational databases (such as Materials Project (Jain et al., 2013) or AFLOW (Curtarolo et al., 2012)) exist, where the collected data are deposited.

The interphase motion of electrons on the illumination of a photo-catalyst (from VB to CB of the semiconductor to the metal particle, participation in a catalytic reaction or recombination) is an inherently dynamic process, occurring on the fs-ns scale. In principle, this requires solving the time-dependent Schrödinger equation (or an equivalent DFT-like approximation) because the ensuing external potential changes with time. A common approach is to use the time-dependent DFT (TD-DFT). When the external perturbation is sufficiently small, the linear-response TD-DFT suffices. The main drawback of the method is its non-trivial computational cost. Hence, it is seldom employed on large (or periodic) systems, constraining its use to small molecules or clusters and thus limiting its descriptive ability considerably.

Although the increasing computational power is about to render this possible, current endeavors usually settle with various tricks of the trade within the conventional DFT (such as constrained DFT (Wu and Van Voorhis, 2005), (Wu and Van Voorhis, 2006) or ΔSCF (Jones and Gunnarsson, 1989), (Hellman et al., 2004), (Gavnholt et al., 2008)) when bothering to deal with the excited states at all.

TD-DFT is still an approximate method. To include the correct physics of various electronic transitions and excited-state theories, multi-reference wave functions are required. This entails costlier approaches, such as using the correlated wavefunction (CW), or Green's function approximation (GW) (Hedin, 1965) and the Bethe–Salpeter equation, and higher multireference coupled-cluster theory (MRCC). The exceeding computational cost can be avoided by splitting the system in the important catalytic center, being treated with high accuracy, and the remainder of the crystal structure. The embedding methods account for the interaction between these parts (Huang et al., 2011), (Yu et al., 2015).

The developed methods currently surpass the available computational capabilities. However, with the available computational power still doubling every two years, as noted by Moore back in 1965 (Moore, 2006), the bottleneck is expected to be overcome before the end of this decade, as 100 FLOP supercomputers will become commonplace. Quantum computers as the next disruptive technology currently range from 10 to 60 qubits and will play a more important role in the next decade.

There is no doubt that photo-thermal catalysis enables kinetic and selectivity benefits that go well beyond those caused by temperature increases at the catalytically active site. The rigorous experiments employing irradiance and wavelength-dependent studies, coupled with kinetic and isotopic analyses provide solid proof of this (Lorber et al., 2022), (Xie et al., 2020), (Tan et al., 2020), (Zhou et al., 2019). However, researchers still too often resort to the perennial explanation of interphase charge transfer which drives the photocatalytic contribution. Despite this assignation (possibly sometimes) being correct, suitable control experiments (*vide supra*) would provide convincing data on how or why the light-induced catalytic effect is happening. These could be utilized to the highest degree possible in terms of maximizing rates or selectivities, or for design of new catalytic materials.

With a systematic approach, the bright future of photo-thermal CO_2 reduction reactions can be brought into reality. The obtained knowledge and methodology (perhaps in part) could also be applied to other reactions, such as artificial photosynthesis and N_2 fixation.

LIMITATIONS OF THE STUDY

The possible role of light on imposing new pathways for photo-catalyst deactivation is seldom investigated. It is known that photo-corrosion can cause detrimental oxidation or reduction of the semiconductors or active metal centers (Wang and Domen, 2020). As a result, long-term photo-thermal experimentation is required to examine the catalyst performance for tens or hundreds of hours and compare the deactivation rates in dark and under illumination. Also, repeating transient dark-light–dark operation mimicking fluctuating solar irradiation brings additional instabilities in the reaction conditions. This can also cause catalytic activity to deteriorate. Such catalytic tests should be performed in conjuction with structural and chemical characterization. The correlation between declined activity and structural changes will enable us to re-engineer and design more stable and robust, not only (initially) very active photo-catalysts.

ACKNOWLEDGMENTS

K.L. and P.D. acknowledge Slovenian Research Agency (ARRS) for funding through program P1-0418 and project J2-1726. Dr. Matej Huš is acknowledged for his helpful contribution related to the theoretical calculations. Dr. Ciara Susan Byrne is kindly acknowledged for language proofreading of this article.

AUTHOR CONTRIBUTIONS

K.L.: Investigation, writing – review & editing, **P.D.:** Conceptualization, investigation, writing – review & editing, funding acquisition.

DECLARATION OF INTERESTS

The authors declare no competing interests.

REFERENCES

Agostini, G., Meira, D., Monte, M., Vitoux, H., Iglesias-Juez, A., Fernández-García, M., Mathon, O., Meunier, F., Berruyer, G., Perrin, F., et al. (2018). XAS/DRIFTS/MS spectroscopy for time-resolved operando investigations at high temperature. J. Synchrotron Radiat. *25*, 1745–1752. https://doi.org/10.1107/S160057751801305X.

Aldana, P.A.U., Ocampo, F., Kobl, K., Louis, B., Thibault-Starzyk, F., Daturi, M., Bazin, P., Thomas, S., and Roger, A.C. (2013). Catalytic CO2 valorization into CH4 on Ni-based ceria-zirconia. reaction mechanism by operando IR spectroscopy. Catal. Today *215*, 201–207. https://doi.org/10.1016/j.cattod.2013.02.019.

Ansari, M.B., and Park, S.-E. (2012). Carbon dioxide utilization as a soft oxidant and promoter in catalysis. Energy Environ. Sci. 9419–9437. https://doi.org/10.1080/09273948.2016.1207785.

Asapu, R., Claes, N., Ciocarlan, R.G., Minjauw, M., Detavernier, C., Cool, P., and Verbruggen, S.W. (2019). Electron transfer and near-field mechanisms in plasmonic gold-nanoparticle-modified TiO2 photocatalytic systems. ACS Appl. Nano Mater. *2*, 4067–4074. https://doi.org/10.1021/acsanm.9b00485.

Aslam, U., Rao, V.G., Chavez, S., Linic, S., and Catalysis, N. (2018). Catalytic conversion of solar to chemical energy on plasmonic metal nanostructures. Nat. Catal. *1*, 656–665. https://doi.org/10.1038/s41929-018-0138-x.

Bansode, A., and Urakawa, A. (2014). Towards full one-pass conversion of carbon dioxide to methanol and methanol-derived products. J. Catal. *309*, 66–70. https://doi.org/10.1016/j.jcat.2013.09.005.

Boll, W., Boll, W., Hochgesand, G., Higman, C., Supp, E., Kalteier, P., Müller, W.D., Kriebel, M., Schlichting, H., and Tanz, H. (2011). Gas production, 3. Gas treating. In Ullmann's Encyclopedia of Industrial Chemistry (Wiley-VCH Verlag GmbH & Co. KGaA), pp. 491–494.

Chang, X., Wang, T., and Gong, J. (2016). CO2 photo-reduction: insights into CO2 activation and reaction on surfaces of photocatalysts. Energy Environ. Sci. *9*, 2177–2196. https://doi.org/10.1039/c6ee00383d.

Cho, Y., Shoji, S., Yamaguchi, A., Hoshina, T., Fujita, T., Abe, H., and Miyauchi, M. (2020). Visible-light-driven dry reforming of methane using a semiconductor-supported catalyst. Chem. Commun. (Camb) *56*, 4611–4614. https://doi.org/10.1039/D0CC00729C.

Collado, L., Reynal, A., Fresno, F., Barawi, M., Escudero, C., Perez-Dieste, V., Coronado, J.M., Serrano, D.P., Durrant, J.R., and de la Peña O'Shea, V.A. (2018). Unravelling the effect of charge dynamics at the plasmonic metal/semiconductor interface for CO2 photoreduction. Nat. Commun. *9*, 4986. https://doi.org/10.1038/s41467-018-07397-2.

Curtarolo, S., Setyawan, W., Wang, S., Xue, J., Yang, K., Taylora, R.H., Nelsond, L.J., Hart, G.L.W., Sanvito, S., Buongiorno-Nardelli, M., et al. (2012). AFLOWLIB.ORG: a distributed materials properties repository from high-throughput ab initio calculations. Comput. Mater. Sci. *58*, 227–235. https://doi.org/10.1016/j.commatsci.2012.02.002.

Darling, G.R., and Holloway, S. (2003). H2 dissociation dynamics on metals: where do we stand? In The Chemical Physics of Solid Surfaces, pp. 27–49. https://doi.org/10.1016/S1571-0785(03)11002-4.

Divins, N.J., Kordus, D., Timoshenko, J., Sinev, I., Zegkinoglou, I., Bergmann, A., Chee, S.W., Widrinna, S., Karslıoğlu, O., Mistry, H., et al. (2021). Operando high-pressure investigation of size-controlled CuZn catalysts for the methanol synthesis reaction. Nat. Commun. *12*, 1435. https://doi.org/10.1038/s41467-021-21604-7.

Djinović, P., Črnivec, I.G.O., Batista, J., Levec, J., and Pintar, A. (2011). Catalytic syngas production from greenhouse gasses: performance comparison of Ru-Al2O3 and Rh-CeO2 catalysts. Chem. Eng. Process. Process Intensification *50*, 1054–1062.

Gargiulo, J., Berté, R., Li, Y., Maier, S.A., and Cortés, E. (2019). From optical to chemical hot spots in plasmonics. Acc. Chem. Res. *52*, 2525–2535. https://doi.org/10.1021/acs.accounts.9b00234.

Gavnholt, J., Thomas, O., Mads, E., and Jakob, S. (2008). Δ self-consistent field method to obtain potential energy surfaces of excited molecules on

surfaces. Phys. Rev. B *78*, 075441. https://doi.org/10.1103/PhysRevB.78.075441.

Ghuman, K.K., Hoch, L.B., Szymanski, P., Loh, J.Y., Kherani, N.P., El-Sayed, M.A., Ozin, G.A., and Singh, C.V. (2016). Photoexcited surface frustrated Lewis pairs for heterogeneous photocatalytic CO2 reduction. J. Am. Chem. Soc. *138*, 1206–1214. https://doi.org/10.1021/jacs.5b10179.

Grabow, L.C., and Mavrikakis, M. (2011). Mechanism of methanol synthesis on Cu through CO2 and CO hydrogenation. ACS Catal. *1*, 365–384. https://doi.org/10.1021/cs200055d.

Graciani, J., Mudiyanselage, K., Xu, F., Baber, A.E., Evans, J., Senanayake, S.D., Stacchiola, D.J., Liu, P., Hrbek, J., Fernández Sanz, J., and Rodriguez, J.A. (2014). Catalysis. Highly active copper-ceria and copper-ceria-titania catalysts for methanol synthesis from CO_2. Science *345*, 546–550. https://doi.org/10.1126/science.1253057.

Han, B., Wei, W., Chang, L., Cheng, P., and Hu, Y.H. (2016). Efficient visible light photocatalytic CO2 reforming of CH4. ACS Catal. *6*, 494–497. https://doi.org/10.1021/acscatal.5b02653.

Han, B., Wei, W., Li, M., Sun, K., and Hu, Y.H. (2019). A thermo-photo hybrid process for steam reforming of methane: highly efficient visible light photocatalysis. Chem. Commun. (Camb) *55*, 7816–7819. https://doi.org/10.1039/c9cc04193a.

He, Y., Yang, K.R., Yu, Z., Fishman, Z.S., Achola, L.A., Tobin, Z.M., Heinlein, J.A., Hu, S., Suib, S.L., Batista, V.S., and Pfefferle, L.D. (2019). Catalytic manganese oxide nanostructures for the reverse water gas shift reaction. Nanoscale *11*, 16677–16688. https://doi.org/10.1039/C9NR06078B.

He, W., Huang, X., Ma, X., and Zhang, J. (2021). Significant temperature effect on the LSPR properties of noble metal nanoparticles. J. Opt. *51*, 142–153. https://doi.org/10.1007/s12596-021-00766-z.

Hedin, L. (1965). New method for calculating the one-particle Green's function with application to the electron-gas problem. Phys. Rev. *139*, A796–A823. https://doi.org/10.1103/PhysRev.139.A796.

Hellman, A., Razaznejad, B., and Lundqvist, B.I. (2004). Potential–energy surfaces for excited states in extended systems. J. Chem. Phys. *120*, 4593–4602. https://doi.org/10.1063/1.1645787.

Hoch, L.B., Wood, T.E., O'Brien, P.G., Liao, K., Reyes, L.M., Mims, C.A., and Ozin, G.A. (2014). The rational design of a single-component photocatalyst for gas-phase CO2 reduction using both UV and visible light. Adv. Sci. (Weinh) *1*, 1400013. https://doi.org/10.1002/advs.201400013.

Huang, C., Pavone, M., and Carter, E.A. (2011). Quantum mechanical embedding theory based on a unique embedding potential. J. Chem. Phys. *134*, 154110. https://doi.org/10.1063/1.3577516.

Jain, A., Ong, S.P., Hautier, G., Chen, W., Richards, W.D., Dacek, S., Cholia, S., Gunter, D., Skinner, D., Ceder, G., and Persson, K.A. (2013). Commentary: the Materials Project: a materials genome approach to accelerating materials innovation. Apl. Mater. *1*, 011002. https://doi.org/10.1063/1.4812323.

Johnston, S.W., and Ahrenkiel, R.K. (1999). Measurement of the temperature-dependent recombination lifetimes in photovoltaic materials. In AIP Conference Proceedings (AIP), pp. 505–510. https://doi.org/10.1063/1.57918.

Jones, R.O., and Gunnarsson, O. (1989). The density functional formalism, its applications and prospects. Rev. Mod. Phys. *61*, 689–746. https://doi.org/10.1103/RevModPhys.61.689.

Kale, M.J., Avanesian, T., and Christopher, P. (2014). Direct photocatalysis by plasmonic nanostructures. ACS Catal. *4*, 116–128. https://doi.org/10.1021/cs400993w.

Karelovic, A., and Ruiz, P. (2013). Mechanistic study of low temperature CO2 methanation over Rh/TiO2 catalysts. J. Catal. *301*, 141–153. https://doi.org/10.1016/j.jcat.2013.02.009.

Kattel, S., Liu, P., and Chen, J.G. (2017). Tuning selectivity of CO2 hydrogenation reactions at the metal/oxide interface. J. Am. Chem. Soc. *139*, 9739–9754. https://doi.org/10.1021/jacs.7b05362.

Kisch, H., and Bahnemann, D. (2015). Best practice in photocatalysis: comparing rates or apparent quantum yields? J. Phys. Chem. Lett. *6*, 1907–1910. https://doi.org/10.1021/acs.jpclett.5b00521.

Kondratenko, E.V., Mul, G., Baltrusaitis, J., Larrazábalc, G.O., and Pérez-Ramírez, J. (2013). Status and perspectives of CO2 conversion into fuels and chemicals by catalytic, photocatalytic and electrocatalytic processes. Energy Environ. Sci. *6*, 3112. https://doi.org/10.1039/c3ee41272e.

Kopač, D., Likozar, B., and Huš, M. (2020). How size matters: electronic, cooperative, and geometric effect in perovskite-supported copper catalysts for CO2 reduction. ACS Catal. *10*, 4092–4102. https://doi.org/10.1021/acscatal.9b05303.

Kumari, G., Kamarudheen, R., Zoethout, E., and Baldi, A. (2021). Photocatalytic surface restructuring in individual silver nanoparticles. ACS Catal. *11*, 3478–3486. https://doi.org/10.1021/acscatal.1c00478.

Kyriakou, V., Vourros, A., Garagounis, I., Carabineiro, S.A.C., Maldonado-Hódar, F.J., Marnellos, G.E., and Konsolakis, M. (2017). Highly active and stable TiO2-supported Au nanoparticles for CO2 reduction. Catal. Commun. *98*, 52–56. https://doi.org/10.1016/j.catcom.2017.05.003.

Lee, D.J., Oh, Y., Hong, J.M., Park, Y.W., and Ju, B.K. (2018). Light sintering of ultra-smooth and robust silver nanowire networks embedded in poly(vinyl-butyral) for flexible OLED. Sci. Rep. *8*, 14170. https://doi.org/10.1038/s41598-018-32590-0.

Li, X., Yu, J., Jaroniec, M., and Chen, X. (2019). Cocatalysts for selective photoreduction of CO2 into solar fuels. Chem. Rev. *119*, 3962–4179. https://doi.org/10.1021/acs.chemrev.8b00400.

Lin, L., Lin, L., Wang, K., Yang, K., Chen, X., Fu, X., and Dai, W. (2017). The visible-light-assisted thermocatalytic methanation of CO2 over Ru/TiO(2-x)Nx. Appl. Catal. B Environ. *204*, 440–455. https://doi.org/10.1016/j.apcatb.2016.11.054.

Liu, L., Zhao, C., and Li, Y. (2012). Spontaneous dissociation of CO2 to CO on defective surface of Cu(I)/TiO2-x nanoparticles at room temperature. J. Phys. Chem. C *116*, 7904–7912. https://doi.org/10.1021/jp300932b.

Liu, H., Thang, M., Dao, D., Liu, Y., Zhou, W., Liu, L., Meng, X., Nagao, T., and Ye, J. (2016). Design of PdAu alloy plasmonic nanoparticles for improved catalytic performance in CO2 reduction with visible light irradiation. Nano Energy *26*, 398–404. https://doi.org/10.1016/j.nanoen.2016.05.045.

Lorber, K., Zavašnik, J., Sancho-Parramon, J., Bubaš, M., Mazaj, M., and Djinović, P. (2022). On the mechanism of visible-light accelerated methane dry reforming reaction over Ni/CeO2−x catalysts. Appl. Catal. B Environ. *301*, 120745. https://doi.org/10.1016/j.apcatb.2021.120745.

Lustemberg, P.G., Ramírez, P.J., Liu, Z., Gutiérrez, R.A., Grinter, D.J., Carrasco, J., Senanayake, S.D., Rodriguez, J.A., and Ganduglia-Pirovano, M.V. (2016). Room-temperature activation of methane and dry reforming with CO2 on Ni-CeO2 (111) surfaces: effect of Ce3+ sites and metal–support interactions on C–H bond cleavage. ACS Catal. *6*, 8184–8191. https://doi.org/10.1021/acscatal.6b02360.

Lustemberg, P.G., Mao, Z., Salcedo, A., Irigoyen, B., Ganduglia-Pirovano, M.V., and Campbell, C.T. (2021). Nature of the active sites on Ni/CeO2 catalysts for methane conversions. ACS Catal. *11*, 10604–10613. https://doi.org/10.1021/acscatal.1c02154.

Marimuthu, A., Zhang, J., and Linic, S. (2013). Tuning selectivity in propylene epoxidation by plasmon mediated photo-switching of Cu oxidation state. Science *339*, 1590–1593. https://doi.org/10.1126/science.1231631.

Martirez, J.M.P., Bao, J.L., and Carter, E.A. (2021). First-principles insights into plasmon-induced catalysis. Annu. Rev. Phys. Chem. *72*, 99–119. https://doi.org/10.1146/annurev-physchem-061020-053501.

Mateo, D., Cerrillo, J.L., Durini, S., and Gascon, J. (2021). Fundamentals and applications of photo-thermal catalysis. Chem. Soc. Rev. *50*, 2173–2210. https://doi.org/10.1039/d0cs00357c.

Melchionna, M., and Fornasiero, P. (2020). Updates on the roadmap for photocatalysis. ACS Catal. *10*, 5493–5501. https://doi.org/10.1021/acscatal.0c01204.

Meng, X., Wang, T., Liu, L., Ouyang, S., Li, P., Hu, H., Kako, T., Iwai, H., Tanaka, A., and Ye, J. (2014). Photothermal conversion of CO2 into CH4 with H2 over group VIII nanocatalysts: an alternative approach for solar fuel production. Angew. Chem. Int. Ed. *53*, 11478–11482. https://doi.org/10.1002/anie.201404953.

Meng, X., Yun, N., and Zhang, Z. (2019). Recent advances in computational photocatalysis: a review. Can. J. Chem. Eng. *97*, 1982–1998. https://doi.org/10.1002/cjce.23477.

Molotskii, M. (2009). Excitonic mechanism of the photoinduced surface restructuring of copper.

Appl. Phys. Lett. *95*, 084103. https://doi.org/10.1063/1.3212727.

Moore, G.E. (2006). Cramming more components onto integrated circuits, Reprinted from Electronics, volume 38, number 8, April 19, 1965, pp.114 ff. IEEE Solid State Circ. Soc. Newsl. *11*, 33–35. https://doi.org/10.1109/N-SSC.2006.4785860.

Mukherjee, S., Libisch, F., Large, N., Neumann, O., Brown, L.V., Cheng, J., Lassiter, J.B., Carter, E.A., Nordlander, P., and Halas, N.J. (2013). Hot electrons do the impossible: plasmon-induced dissociation of H2 on Au. Nano Lett. *13*, 240–247. https://doi.org/10.1021/nl303940z.

Muroyama, H., Tsuda, Y., Asakoshi, T., Masitah, H., Okanishi, T., Matsui, T., and Eguchi, K. (2016). Carbon dioxide methanation over Ni catalysts supported on various metal oxides. J. Catal. *343*, 178–184. https://doi.org/10.1016/j.jcat.2016.07.018.

Muñoz-Batista, M.J., Meira, D.M., Colón, G., Kubacka, A., and Fernández-García, M. (2018). Phase-contact engineering in mono- and bimetallic Cu-Ni Co-catalysts for hydrogen photocatalytic materials. Angew. Chem. Int. Ed. *57*, 1199–1203. https://doi.org/10.1002/anie.201709552.

Nakamura, J., Fujitani, T., Kuld, S., Helveg, S., Chorkendorff, I., and Sehested, J. (2017). Comment on "Active sites for CO2 hydrogenation to methanol on Cu/ZnO catalysts". Science *357*, eaan8074. https://doi.org/10.1126/science.aan8074.

Oba, F., and Kumagai, Y. (2018). Design and exploration of semiconductors from first principles: a review of recent advances. Appl. Phys. Express *11*, 060101. https://doi.org/10.7567/APEX.11.060101.

Ott, J., Gronemann, V., Pontzen, F., Fiedler, E., Grossmann, G., Kersebohm, D.B., Weiss, G., and Witte, C. (2012). Methanol. In Ullmann's Encyclopedia of Industrial Chemistry (Wiley-VCH Verlag GmbH & Co. KGaA), pp. 6–12.

Pan, Q., Peng, J., Wang, S., and Wang, S. (2014). In situ FTIR spectroscopic study of the CO2 methanation mechanism on Ni/Ce0.5Zr 0.5O2. Catal. Sci. Technol. *4*, 502–509. https://doi.org/10.1039/C3CY00868A.

Porosoff, M.D., Yan, B., and Chen, J.G. (2016). Catalytic reduction of CO2 by H2 for synthesis of CO, methanol and hydrocarbons: challenges and opportunities. Energy Environ. Sci. *9*, 62–73. https://doi.org/10.1039/C5EE02657A.

Schwab, E., Milanov, A., Schunk, S.A., Behrens, A., and Schödel, N. (2015). Dry reforming and reverse water gas shift: alternatives for syngas production? Chem. Ing. Tech. *87*, 347–353. https://doi.org/10.1002/cite.201400111.

Shi, W., Guo, X., Cui, C., Jiang, K., Li, Z., Qu, L., and Wang, J.C. (2019). Controllable synthesis of Cu2O decorated WO3 nanosheets with dominant (0 0 1) facets for photocatalytic CO2 reduction under visible-light irradiation. Appl. Catal. B Environ. *243*, 236–242. https://doi.org/10.1016/j.apcatb.2018.09.076.

Shoji, S., Peng, X., Yamaguchi, A., Watanabe, R., Fukuhara, C., Cho, Y., and Miyauchi, M. (2020a). Photocatalytic uphill conversion of natural gas beyond the limitation of thermal reaction systems. Nat. Catal. *3*, 148–153. https://doi.org/10.1038/s41929-019-0419-z.

Shoji, S., Peng, X., Yamaguchi, A., Watanabe, R., Fukuhara, C., Cho, Y., and Miyauchi, M. (2020b). Photocatalytic uphill conversion of natural gas beyond the limitation of thermal reaction systems. Nat. Catal. *3*, 148–153. https://doi.org/10.1038/s41929-019-0419-z.

Solis-Garcia, A., Louvier-Hernandez, J.F., Almendarez-Camarillo, A., and Fierro-Gonzalez, J.C. (2017). Participation of surface bicarbonate, formate and methoxy species in the carbon dioxide methanation catalyzed by ZrO2-supported Ni. Appl. Catal. B Environ. *218*, 611–620. https://doi.org/10.1016/j.apcatb.2017.06.063.

Song, H., Meng, X., Dao, T.D., Zhou, W., Liu, H., Shi, L., Zhang, H., Nagao, T., Kako, T., and Ye, J. (2018a). Light-enhanced carbon dioxide activation and conversion by effective plasmonic coupling effect of Pt and Au nanoparticles. ACS Appl. Mater. Inter. *10*, 408–416. https://doi.org/10.1021/acsami.7b13043.

Song, H., Meng, X., Wang, Z.J., Wang, Z., Chen, H., Weng, Y., Ichihara, F., Oshikiri, M., Kako, T., and Ye, J. (2018b). Visible-light-mediated methane activation for steam methane reforming under mild conditions: a case study of Rh/TiO2 catalysts. ACS Catal. Am. Chem. Soc. *8*, 7556–7565. https://doi.org/10.1021/acscatal.8b01787.

Song, C., Liu, X., Xu, M., Masi, D., Wang, Y., Deng, Y., and Ma, D. (2020). Photothermal conversion of CO2 with tunable selectivity using Fe-based catalysts: from oxide to carbide. ACS Catal. *10*, 10364–10374. https://doi.org/10.1021/acscatal.0c02244.

Su, Y.Q., Filot, I.A.W., Liu, J.X., and Hensen, E.J.M. (2018). Stable Pd-doped ceria structures for CH4 activation and CO oxidation. ACS Catal. *8*, 75–80. https://doi.org/10.1021/acscatal.7b03295.

Tahir, B., Tahir, M., and Amin, N.S. (2015). Gold–indium modified TiO2 nanocatalysts for photocatalytic CO2 reduction with H2 as reductant in a monolith photoreactor. Appl. Surf. Sci. *338*, 1–14. https://doi.org/10.1016/j.apsusc.2015.02.126.

Tan, T.H., Xie, B., Ng, Y.H., Abdullah, S.F.B., Tang, H.Y.M., Bedford, N., and Scott, J. (2020). Unlocking the potential of the formate pathway in the photo-assisted Sabatier reaction. Nat. Catal. *3*, 1034–1043. https://doi.org/10.1038/s41929-020-00544-3.

Van Hardeveld, R., and Hartog, F. (1969). The statistics of surface atoms and surface sites on metal crystals. Surf. Sci. *15*, 189–230. https://doi.org/10.1016/0039-6028(69)90148-4.

Vasiliades, M.A., Djinović, P., Pintar, A., Kovač, J., and Efstathiou, A.M. (2017). The effect of CeO2 –ZrO2 structural differences on the origin and reactivity of carbon formed during methane dry reforming over NiCo/CeO2 –ZrO2 catalysts studied by transient techniques. Catal. Sci. Technol. *7*, 5422–5434. https://doi.org/10.1039/C7CY01009E.

Vogt, C., Monai, M., Sterk, E.B., Palle, J., Melcherts, A.E.M., Zijlstra, B., Groeneveld, E., Berben, P.H., Boereboom, J.M., Hensen, E.J.M., et al. (2019). Understanding carbon dioxide activation and carbon-carbon coupling over nickel. Nat. Commun. *10*, 5330. https://doi.org/10.1038/s41467-019-12858-3.

Vogt, C., Vogt, C., Kranenborg, J., Monai, M., and Weckhuysen, B.M. (2020). Structure sensitivity in steam and dry methane reforming over nickel: activity and carbon formation. ACS Catal. Am. Chem. Soc. *10*, 1428–1438. https://doi.org/10.1021/acscatal.9b04193.

Vovchok, D., Zhang, C., Hwang, S., Jiao, L., Zhang, F., Liu, Z., and Rodriguez, J.A. (2020). Deciphering dynamic structural and mechanistic complexity in Cu/CeO2/ZSM-5 catalysts for the reverse water-gas shift reaction. ACS Catal. *10*, 10216–10228. https://doi.org/10.1021/acscatal.0c01584.

Vrijburg, W.L., Moioli, E., Chen, W., Zhang, M., Terlingen, B.J., Zijlstra, B., and Hensen, E.J. (2019). Efficient base-metal NiMn/TiO2 catalyst for CO2 methanation. ACS Catal. *9*, 7823–7839. https://doi.org/10.1021/acscatal.9b01968.

Wang, Q., and Domen, K. (2020). Particulate photocatalysts for light-driven water splitting: mechanisms, challenges, and design strategies. Chem. Rev. *120*, 919–985. https://doi.org/10.1021/acs.chemrev.9b00201.

Wang, L., Ghoussoub, M., Wang, H., Shao, Y., Sun, W., Tountas, A.A., and Ozin, G.A. (2018). Photocatalytic hydrogenation of carbon dioxide with high selectivity to methanol at atmospheric pressure. Joule *2*, 1369–1381. https://doi.org/10.1016/j.joule.2018.03.007.

Wang, K., Jiang, R., Peng, T., Chen, X., Dai, W., and Fu, X. (2019a). Modeling the effect of Cu doped TiO2 with carbon dots on CO2 methanation by H2O in a photo-thermal system. Appl. Catal. B Environ. *256*, 117780. https://doi.org/10.1016/j.apcatb.2019.117780.

Wang, Z., Wang, Z.J., Song, H., Pang, H., Ning, Y., Dao, T.D., Wang, Z., and Ye, J. (2019b). Photo-assisted methanol synthesis via CO2 reduction under ambient pressure over plasmonic Cu/ZnO catalysts. Appl. Catal. B Environ. *250*, 10–16. https://doi.org/10.1016/j.apcatb.2019.03.003.

Wang, Z.J., Song, H., Liu, H., and Ye, J. (2020). Coupling of solar energy and thermal energy for carbon dioxide reduction: status and prospects. Angew. Chem. Int. Ed. Engl. *59*, 8016–8035. https://doi.org/10.1002/anie.201907443.

Weckhuysen Research Group Website (2021). https://bertweckhuysen.com/equipment-2/.

Wei, J., and Iglesia, E. (2004). Isotopic and kinetic assessment of the mechanism of reactions of CH4 with CO2 or H2O to form synthesis gas and carbon on nickel catalysts. J. Catal. *224*, 370–383. https://doi.org/10.1016/j.jcat.2004.02.032.

Wilkinson, S.K., Van De Water, L.G.A., Miller, B., Simmons, M.J.H., Stitt, E.H., and Watson, M.J. (2016). Understanding the generation of methanol synthesis and water gas shift activity over copper-based catalysts-A spatially resolved experimental kinetic study using steady and non-steady state operation under CO/CO2/H2 feeds.

J. Catal. *337*, 208–220. https://doi.org/10.1016/j.jcat.2016.01.025.

Williams, W.D., Williams, W.D., Greeley, J.P., Delgass, W.N., and Ribeiro, F.H. (2017). Water activation and carbon monoxide coverage effects on maximum rates for low temperature water-gas shift catalysis. J. Catal. *347*, 197–204. https://doi.org/10.1016/j.jcat.2017.01.016.

Wu, Q., and Van Voorhis, T. (2005). Direct optimization method to study constrained systems within density-functional theory. Phys. Rev. A *72*, 024502. https://doi.org/10.1103/PhysRevA.72.024502.

Wu, Q., and Van Voorhis, T. (2006). Direct calculation of electron transfer parameters through constrained density functional theory. J. Phys. Chem. A *110*, 9212–9218. https://doi.org/10.1021/jp061848y.

Xie, Z., Liao, Q., Liu, M., Yang, Z., and Zhang, L. (2017). Micro-kinetic modeling study of dry reforming of methane over the Ni-based catalyst. Energy Convers. Manag. *153*, 526–537. https://doi.org/10.1016/j.enconman.2017.10.022.

Xie, B., Wong, R.J., Tan, T.H., Higham, M., Gibson, E.K., Decarolis, D., Callison, J., Aguey-Zinsou, K.F., Bowker, M., Catlow, C.R.A., et al. (2020). Synergistic ultraviolet and visible light photo-activation enables intensified low-temperature methanol synthesis over copper/zinc oxide/alumina. Nat. Commun. *11*, 1615. https://doi.org/10.1038/s41467-020-15445-z.

Xie, B., Kumar, P., Tan, T.H., Esmailpour, A.A., Aguey-Zinsou, K.F., Scott, J., and Amal, R. (2021). Doping-mediated metal–support interaction promotion toward light-assisted methanol production over Cu/ZnO/Al2O3. ACS Catal. *11*, 5818–5828. https://doi.org/10.1021/acscatal.1c00332.

Xiong, W., Gu, X.K., Zhang, Z., Chai, P., Zang, Y., Yu, Z., Li, D., Zhang, H., Liu, Z., and Huang, W. (2021). Fine cubic Cu2O nanocrystals as highly selective catalyst for propylene epoxidation with molecular oxygen. Nat. Commun. *12*, 5921. https://doi.org/10.1038/s41467-021-26257-0.

Yang, Z., Yang, Z., Zeng, M., Wang, K., Yue, X., Chen, X., Dai, W., and Fu, X. (2022). Visible light-assisted thermal catalytic reverse water gas reaction over Cu-CeO2: the synergistic of hot electrons and oxygen vacancies induced by LSPR effect. Fuel *315*, 123186. https://doi.org/10.1016/j.fuel.2022.123186.

Yu, K., Libisch, F., and Carter, E.A. (2015). Implementation of density functional embedding theory within the projector-augmented-wave method and applications to semiconductor defect states. J. Chem. Phys. *143*, 102806. https://doi.org/10.1063/1.4922260.

Zabilskiy, M., Sushkevich, V.L., Palagin, D., Newton, M.A., Krumeich, F., and van Bokhoven, J.A. (2020). The unique interplay between copper and zinc during catalytic carbon dioxide hydrogenation to methanol. Nat. Commun. *11*, 2409. https://doi.org/10.1038/s41467-020-16342-1.

Zhang, F., Liu, Z., Chen, X., Rui, N., Betancourt, L.E., Lin, L., Xu, W., Sun, C., Abeykoon, A.M.M., Rodriguez, J.A., et al. (2020). The effects of Zr-doping into ceria for the dry reforming of methane over Ni/CeZrO2 catalysts: in-situ studies with XRD, XAFS and AP-XPS. ACS Catal. *10*, 3274–3284. https://doi.org/10.1021/acscatal.9b04451.

Zhou, L., Swearer, D.F., Robatjazi, H., Alabastri, A., Christopher, P., Carter, E.A., Nordlander, P., and Halas, N.J. (2019). Response to Comment on "Quantifying hot carrier and thermal contributions in plasmonic photocatalysis". Science *364*, 69–72. https://doi.org/10.1126/science.aaw9545.

Zhou, L., Zhou, L., Martirez, J.M.P., Finzel, J., Zhang, C., Swearer, D.F., Tian, S., and Halas, N.J. (2020). Light-driven methane dry reforming with single atomic site antenna-reactor plasmonic photocatalysts. Nat. Energy *5*, 61–70. https://doi.org/10.1038/s41560-019-0517-9.